Water Research 183 (2020) 116081

Contents lists available at ScienceDirect

Water Research

journal homepage: www.elsevier.com/locate/watres

Similar retardation of arsenic in gray Holocene and orange Pleistocene sediments: Evidence from field-based column experiments in Bangladesh

M. Rajib H. Mozumder [a, b, *], Benjamin C. Bostick [a], Magdi Selim [c], M. Atikul Islam [d], Elizabeth M. Shoenfelt [a, e], Tyler Ellis [a], Brian J. Mailloux [f], Imtiaz Choudhury [d], Kazi M. Ahmed [d], Alexander van Geen [a]

[a] Lamont-Doherty Earth Observatory of Columbia University, NY, 10964, USA
[b] Now at Gradient, One Beacon Street, 17th Floor, Boston, MA, 02108, USA
[c] School of Plant, Environmental, and Soil Sciences, Louisiana State University AgCenter, Baton Rouge, LA, 70803, USA
[d] Department of Geology, University of Dhaka, Dhaka, 1000, Bangladesh
[e] Now at Department of Earth, Atmospheric, and Planetary Sciences, Massachusetts Institute of Technology, Cambridge, MA, 02139, USA
[f] Environmental Science, Barnard College, New York, NY, 10027, USA

ARTICLE INFO

Article history:
Received 9 March 2020
Received in revised form
15 June 2020
Accepted 16 June 2020
Available online 18 June 2020

Keywords:
Arsenic
Groundwater
Transport
Column experiment
Kinetic model
Bangladesh

ABSTRACT

Groundwater flow has the potential to introduce arsenic (As) in previously uncontaminated aquifers. The extent to which As transport is retarded by adsorption is particularly relevant in Bangladesh where low-As wells offer the best chance of reducing chronic exposure to As of a large rural population dependent on groundwater. In this study, column experiments were conducted with intact cores in the field to measure As retardation. Freshly collected cores of reduced iron (Fe-II) dominated gray sediment of Holocene age as well as oxidized Fe (III)-coated orange sediment of Pleistocene age were eluted at pore-water velocities of 40–230 cm/day with anoxic groundwater pumped directly from a well and containing 320 μg/L As. Up to 100 μg/L As was immediately released from gray sand but the main As breakthrough for both gray and orange sand occurred between 30 and 70 pore volumes, depending on flow rate. The early release of As from gray sand is attributed to the presence of a weakly bound pool of As. The sorption of As was kinetically limited in both gray and orange sand columns. We used a reversible multi-reaction transport model to simulate As breakthrough curves while keeping the model parameters as constant as possible. Contrary to the notion that dissolved As is sorbed more strongly to orange sands, we show that As was similarly retarded in both gray and orange sands in the field.

1. Introduction

Millions of people in South and Southeast Asia drink groundwater pumped from low-As (<10 μg/L) alluvial aquifers, typically composed of oxidized, Fe(III) oxide coated orange sediment of Pleistocene age (DPHE/BGS, 2001; Ravenscroft et al., 2009; Fendorf et al., 2010). These aquifers are often in close proximity to high-As, anoxic Holocene aquifers composed of gray sediment, often containing naturally elevated levels of As (>100 μg/L) released by the microbial reduction of iron(oxy)hydroxides (Bhattacharya et al., 1997; Nickson et al., 1998; DPHE/BGS, 2001; Berg et al., 2001; Ahmed et al., 2004). Low-As aquifers can be contaminated by flow from high-As aquifers, but migration of As is affected by sorption to sediments during groundwater flow (Ravenscroft et al., 2009). Understanding the partitioning of As between groundwater and aquifer sediment that contain a sizeable pool (<1–5 mg/kg) of adsorbed As (Zheng et al., 2005; van Geen et al., 2008) is, therefore, important to predict the vulnerability of low-As aquifers.

The partitioning of As between the solid and aqueous phase is often described using an empirical partition coefficient K_D, the ratio of the As concentration in the solid phase divided by the As concentration in the dissolved phase. This approximation is useful to describe transport under near-equilibrium and stable conditions

* Corresponding author. Lamont-Doherty Earth Observatory of Columbia University, NY, 10964, USA
E-mail addresses: mhm2160@columbia.edu, rmozumder@gradientcorp.com (M.R.H. Mozumder).

https://doi.org/10.1016/j.watres.2020.116081
0043-1354/

(Baes and Sharp, 1983). K_D estimates are affected by groundwater pH, competing oxyanions such as phosphate, bicarbonate, and silicate, the oxidation state of As, and sediment mineralogy (Smedley and Kinniburgh, 2002; Dixit and Hering, 2003; Thi Hoa Mai et al., 2014). The equilibrium assumption is less appropriate when groundwater flow is accelerated, for example, by pumping for irrigation or the municipal supply of large cities (Michael and Voss, 2008; Knappett et al., 2016; Khan et al., 2016; Mozumder et al., 2020; Mihajlov et al., 2020). Indeed, recent laboratory and field studies have suggested that As transport is a non-equilibrium or rate-limited process (Darland and Inskeep, 1997; Zhang and Selim, 2005, 2008; Selim, 2014). Despite these limitations, a K_D can still be useful to predict As transport in aquifers where groundwater velocities are relatively well constrained by field measurements of environmental tracers/isotopes in groundwater (Mozumder et al., 2020).

In gray Holocene sediment, As is thought to be efficiently transported because few sorption sites are available for As (Harvey et al., 2002; Swartz et al., 2004). However, laboratory and field experiments suggest adsorption can still occur in gray sand aquifers (DPHE/BGS, 2001; Harvey et al., 2002; Swartz et al., 2004; van Geen et al., 2008; Itai et al., 2010; Jung et al., 2012; Thi Hoa Mai et al., 2014; Radloff et al., 2015). The wide range of K_D values of 0.15–46 L/kg derived from these experiments corresponds to retardation factors of 2–300, assuming an aquifer material bulk density of 1.8 g/cm^3 and a porosity of 30%. It is unclear to what extent this reflects variations in experimental conditions (e.g. duration of experiment), sediment properties or preservation, or other factors such as kinetic limitations that prevent equilibrium adsorption-desorption.

The extent of adsorption of As to orange sediments may differ from adsorption to gray sands and thought to provide significant protection against the intrusion of high As groundwater (Stollenwerk et al., 2007; McArthur et al., 2011; Robinson et al., 2011; Radloff et al., 2011; van Geen et al., 2013). Laboratory studies conducted in batch mode generally indicate higher K_D values (20–70 L/kg; retardation of 120–420) in orange compared to gray sands. Some of these laboratory experiments may have been affected by sediment storage, repacking of sediment, and the use of artificial groundwater that is not representative of field conditions. Field-based studies, on the other hand, are not affected by storage but are subject to different uncertainties such as aquifer mineralogy, groundwater composition, and the direction/rate of groundwater flow. Field studies often indicate a lower K_D of 1–10 L/kg for originally orange sand that, in some cases, turned gray (Mihajlov et al., 2020) and therefore lower retardation factors of 7–60 (McArthur et al., 2011; Radloff et al., 2011; van Geen et al., 2013).

Here, we used a novel hybrid of field- and experimental research to study As transport in gray and orange sediments reacted with anaerobic groundwater under ambient conditions. The fresh sediments used are from intact cores to ensure that their sediment microbial community, mineralogy and redox-state are unaffected by storage. High-As, anoxic groundwater pumped directly from a shallow well was eluted for the present study at different rates through a series of columns containing intact, fresh gray and orange aquifer sediment and monitored in the field under anaerobic conditions. We hypothesized when designing this study that orange sands would show greater retention than gray sands and thus more effectively protect low-As aquifers from the intrusion of As-containing groundwater. The need for a reliable measure of As retention in both reduced gray- and oxidized orange-sands to assess the long-term vulnerability and sustainability of low-As aquifers motivated the study.

2. Material and methods

2.1. Sediment coring and column preparation

Sediment cores containing Holocene gray sand and Pleistocene orange sand were collected in Araihazar, Bangladesh, immediately before the experiment (Fig. 1). Intact cores were retrieved (30 cm long, 1.8 cm outer diameter) using a hammer-driven soil corer (AMS 424.45) from drilling depths between 12.2 and 18.3 m. Immediately after retrieval, the cores were refrigerated in nitrogen-flushed Mylar bags that were heat-sealed after adding oxygen absorbers (IMPAK sorbent systems). Within 24 h, and inside a nitrogen-inflated glove chamber (Glas-Col04408-38), a total of 15 undisturbed sediment columns (8 gray and 7 orange sediment columns), 7.5 cm in length and 1.6 cm in diameter, were prepared from the central portion of the recovered cores using a precision tube cutter. The inlets and outlets of the columns were enclosed with custom-made plugs after inserting a thin layer of glass wool to prevent the loss of fine particles. A column packed with pure sand (ACROS Organics 370942500) was prepared in parallel as a control.

2.2. Experimental setup

The gray and orange sediment columns along with a sand column containing 99.8% SiO_2 (Quartz) and ~0.01% iron oxide (mesh size: 40–100) were eluted with groundwater directly at the wellhead from a shallow well screened from 18 to 20 m, a depth where As concentrations typically peak in the study area (Fig. S1c). The influent groundwater from the shallow well was pumped continuously at a rate of 8 L/min into a bag (50 L capacity) shaped like a pyramid that was kept overflowing through a narrow opening at the top to ensure a constant supply of anoxic groundwater (Fig. 2). The storage bag was placed at a higher elevation than the columns to ensure uninterrupted, steady flow in the event of a pump stoppage or electricity failure. The custom-made bag (Ready Containment LLC) facilitated escape of gas bubbles that tend to cling to the corners of a regular container. Groundwater from the storage bag reached a manifold that divided the flow into the columns at different rates using peristaltic pumps (Gilson Minipuls 3) and various tubing diameters. The columns were housed in custom-made anoxic chambers (modified Becton-Dickinson#260672) with pouches that consume oxygen (Becton-Dickinson#260678) and anaerobic indicator strips (Becton-Dickinson#271051). The columns were placed inside the chamber in their natural orientation, with the groundwater entering the top of each column (Fig. 2), and with sufficient backpressure to prevent gravity flow and degassing.

Of the experiments performed, a total of 10 sediment columns (6 gray and 4 orange sand columns) were successfully completed, and 5 were compromised due to repeated flow interruption. We focus here on the 10 successful columns. Most of the columns ($n = 8$) were eluted either at an average pore water velocity (PWV) of 154 ± 10 cm/day or 75 ± 10 cm/day. In addition, one orange sand column was eluted at 40 cm/day and one column of gray sand was eluted at 230 cm/day (Table 1).

2.3. Sampling and onsite measurements

Column effluents were collected in a manually operated fraction collector in acid leached (10% HCl) 15 ml vials every 1-3 h for the first 10 days of the experiment, followed by every 12 h for 2 weeks. The sample volume was documented at the time of collection. Every other sample was acidified in the field with TraceMetal grade HCl. Some of the remaining samples remained unacidified for anion analysis while others were acidified later in the lab with Optima

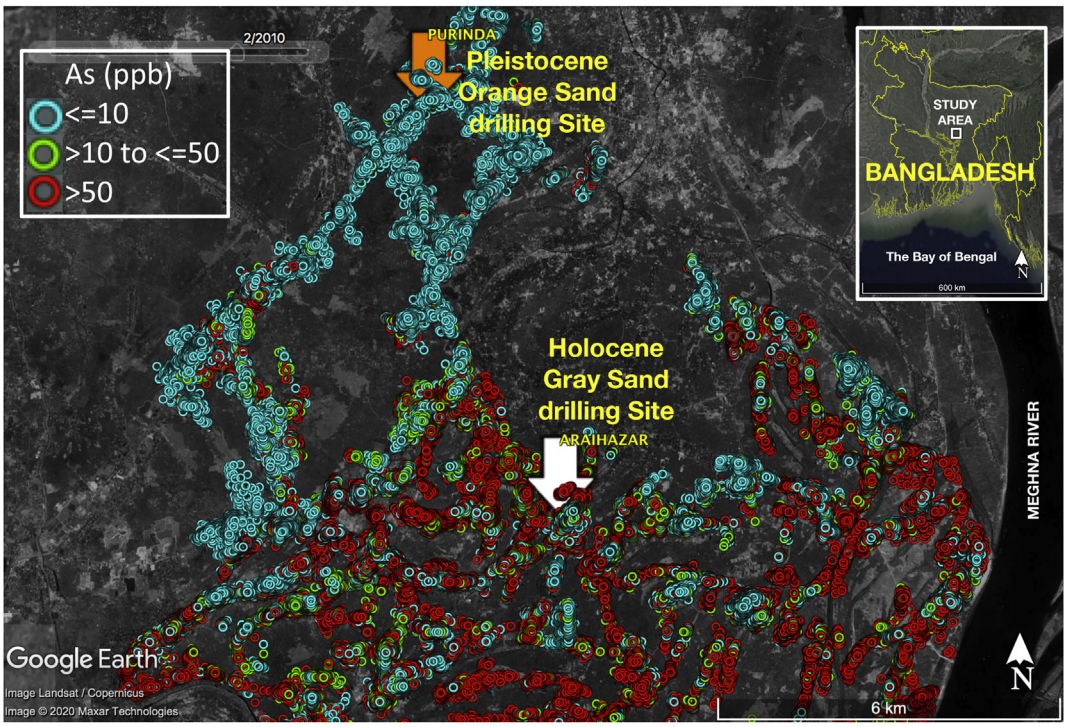

Fig. 1. Study Area. A Google Earth map indicates the location of drilling sites in the Araihazar Upazila of central Bangladesh (inset). Also shown is the spatial distribution of As concentrations in Araihazar based on a field-testing campaign (van Geen et al., 2014) grouped into ≤ 10 μg/L (cyan), >10 to 50 μg/L (green), and >50 μg/L (red). Shallow orange sediments were cored in the NW part of the area (90.6352°, 23.8542°) with a higher proportion of low As wells (<10 μg/L) tapping the Pleistocene aquifer. The gray sediments were cored from a highly As-contaminated area in central Araihazar (90.6577°, 23.7909°).

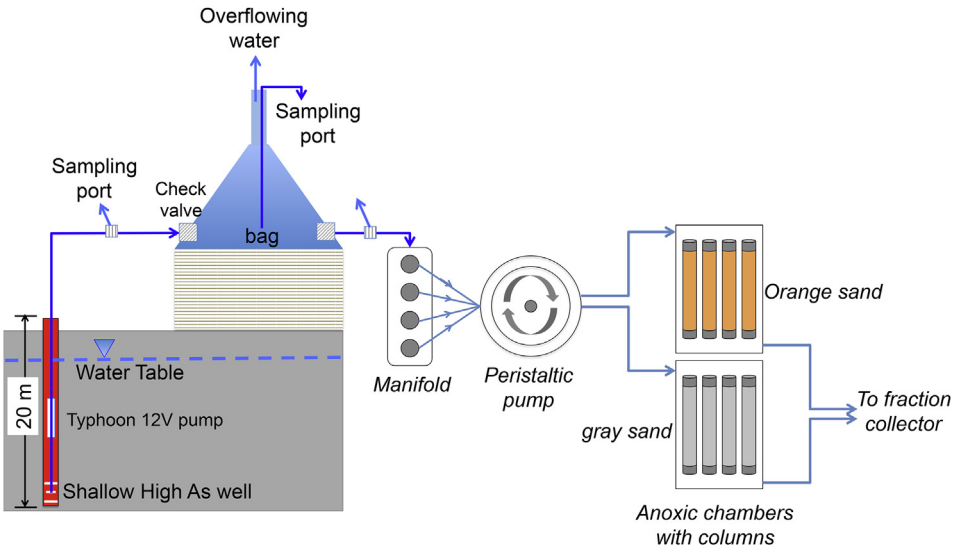

Fig. 2. A schematic of the experimental setup. High arsenic groundwater from the shallow aquifer was pumped continuously in an overflowing bag and channeled under controlled flow rates to elute undisturbed sediment cores housed in custom made anoxic chambers. The figure is not drawn to scale.

grade HCl for cation analysis. After 20 days, groundwater flow into the storage bag was interrupted and the retained water in the bag was spiked with sodium bromide (Fisher#S255-500) at about 120 mg/L and sodium phosphate monobasic dihydrate (Fisher #S381-500) at about 6 mg/L (Fig. S2d and h). The purpose of spiking with bromide and phosphate was to characterize sediment porosity and column dispersion and the effect of phosphate exchange, respectively.

The influent groundwater was sampled daily at an outlet before it reached the storage bag and from the bottom of the storage bag (Fig. 2). Dissolved oxygen concentration in the influent water was tested daily with a visual kit (Chemetrics 0–40 ppb). The input water was also monitored daily for pH, ORP (oxidation-reduction potential), electrical conductivity, and temperature using Oakton probes (UX-35650-10 and UX-35634-30). A pH flow-through cell (UX-05662-48) was used to measure pH in a subset of column effluents. Arsenic speciation cartridges were used in the field to separate As(V) from As(III) in the influent water as well as in a

Table 1
Column transport parameters for gray and orange sediments.

Core depth	Dry weight	Column length	Volume	Bulk Density	Porosity	Pore volume (PV)	Darcy's flux	Pore water velocity (PWV)
meter	g	cm	cm^3	g/cm^3	cm^3/cm^3	mL	cm/hr	cm/day
Holocene gray sediment columns								
14	27.4	7.5	15.1	1.82	0.31	4.72	3.0	230*
15.2	27.4	7.5	15.1	1.82	0.31	4.74	2.0	156*
15.4	26.2	7.5	15.1	1.74	0.34	5.18	2.0	140
15	26.6	7.0	14.1	1.89	0.29	4.03	2.0	165
17.2	28.3	7.5	15.1	1.88	0.29	4.41	0.8	66*
13.5	28.8	7.5	15.1	1.91	0.28	4.23	0.9	73
Pleistocene orange sediment columns								
13.7	27.6	7.5	15.1	1.83	0.31	4.67	2.0	155*
12.8	29.2	7.8	15.7	1.86	0.30	4.66	1.0	81*
13	27.0	7.5	15.1	1.79	0.32	4.89	1.1	81
15.5	27.9	7.5	15.1	1.85	0.30	4.56	0.5	40

* Sediment columns used to model As breakthrough in Fig. 6.

subset of column effluents immediately after collection (Meng et al., 2001). Samples for dissolved organic carbon (DOC) and dissolved inorganic carbon (DIC) were collected in 22 ml clear glass vials (Sigma-Aldrich 27173 Supelco). The DOC samples were acidified to 0.1% HCl while DIC samples were left unacidified.

2.4. Sediment analyses

2.4.1. Reflectance spectroscopy

Sediment cuttings collected while drilling were packed in plastic Saran wrap. A Konica Minolta CM-600d spectrophotometer was used to measure the difference in diffuse spectral reflectance between 530 and 520 nm (Horneman et al., 2004) through the plastic wrap soon after the samples were collected, as a proxy for the redox state of surficial Fe oxides (Fig. S1a-b). Measurements were made in triplicate by the spectrophotometer and recorded for three different spots on each sample of cuttings.

2.4.2. X-ray fluorescence (XRF) and sediment phosphate extraction

The Saran-wrapped sediment cuttings were also analyzed with a handheld X-ray fluorescence analyzer (InnovX Delta) in 3-beam soil mode for bulk As concentration (Table 2). The internal calibration of the instrument was verified by analyzing reference NIST standards (SRM 2709, 2710, and 2711) in between samples. As a measure of the exchangeable As content of the sediment, 1 g of sand (n = 8) immersed in 55 ml N_2-flushed 1 M Na_2HPO_4 solution was adjusted to a pH of 5 for 24 h (Zheng et al., 2005). The extraction was conducted in an anaerobic chamber (Coy#120001) and the solutions were filtered through 0.45 μm media.

Table 2
Bulk chemical properties of the gray and orange sediments.

Coring depth	As (total)	P-ext. As	P-ext. As	Ca	Fe (total)
(m)	(mg/kg)	(mg/kg)	(%)	(g/kg)	(%)[a]
Holocene gray sediment cuttings					
10.7	2.4 ± 0.6			8.3 ± 0.15	1.8
12.2	–			9.6 ± 0.15	1.7
13.7	4.2 ± 0.6			5.8 ± 0.12	2.1
15.2	–			3.5 ± 0.09	0.8
16.8	2.1 ± 0.5			8.6 ± 0.14	1.2
18.2	2.4 ± 0.5			5.3 ± 0.11	1.1
18.2	–			6.5 ± 0.12	1.2
19.8	1.9 ± 0.5	0.44	23.1	7.5 ± 0.13	1.1
12.8	1[b] ± 1.6	0.70	70.5	6.2 ± 0.12	1.6
–	2.4 ± 0.5	0.99	41.2	8.9 ± 0.15	1.3
16.5	4.1 ± 0.6	1.68	40.9	6.1 ± 0.13	2.9
Average	3 ± 0.6	1 ± 0.5	44 ± 20	6.9 ± 0.13	1.5
Pleistocene orange sediment cuttings					
12.8	–			3.4 ± 0.1	2.4
12.8	–			3.6 ± 0.11	2.4
13	3 ± 0.5			4.5 ± 0.11	2.5
13	–			5 ± 0.12	3.2
13.7	–			4.4 ± 0.12	3.8
14	2.6 ± 0.6			4.5 ± 0.11	2.1
15.5	2.1 ± 0.6			4.7 ± 0.11	3.0
12.5	2.8 ± 0.6	0.27	9.7	2.5 ± 0.09	1.9
14.6	1.8 ± 0.6	0.29	16.4	4.6 ± 0.11	2.0
15.2	2.3 ± 0.6	0.47	20.4	4.9 ± 0.12	2.8
13.5	1.8 ± 0.6	0.27	14.9	5.2 ± 0.12	2.6
Average	2 ± 0.6	0.3 ± 0.1	15 ± 4	4.4 ± 0.11	2.4

[a] 1% Fe = 10,000 mg/kg.
[b] Not included for averaging because the minimum detection limit of the handheld XRF was assumed.

2.4.3. X-ray absorption spectroscopy (XAS)

Iron (Fe) K-edge X-ray absorption spectra were collected on pristine gray and orange sediment cuttings in fluorescence mode at the Stanford Synchrotron Radiation Lightsource (SSRL) on beamlines 4–1 and 11–2. Fe spectra were collected using either 32 or 100-element Ge detectors windowed on the Fe K_α fluorescence peak, using a 3μx Mn filter. Spectra were calibrated using a Fe metal foil (7112.0 eV). No photooxidation or reduction was observed during data collection.

Spectral analysis was performed as detailed in Shoenfelt et al. (2018). Fe(II) content and mineral composition were determined by linear combination fitting using a combination of five (of 10) reference compounds (pyrite, siderite, goethite, hematite, magnetite, biotite, augite, hornblende, nontronite, ferrihydrite) that produced the best fit. This approach is effective at identifying major or more distinct minerals but less abundant minerals may be omitted from fits even when present at concentrations less than 10%. Silicate minerals are often similar, so nontronite and biotite should be regarded as trioctahedral Fe(III) and dioctahedral Fe(II) phyllosilicates, and augite fits are representative of Fe(II/III) silicates including hornblende. Errors in mineral composition, usually within 5% of total Fe, are based on sensitivity analysis and fitting quality (Newville, 2001). This method is effective for most iron minerals, but combines ferrihydrite and nanocrystalline goethite into a single, reactive Fe(III)oxyhydroxide group (Sun et al., 2018).

2.5. Analyses of groundwater and sediment extracts

All acidified (1% HCl) samples collected from the input well, storage tank, column effluents, and sediment extracts were analyzed for P, S, Fe, Mn, As, Na, K, Ca, Mg, Ba, and Sr using high-resolution inductively coupled plasma-mass spectrometry (HR ICP-MS) with a detection limit of 0.1 μg/L accounting for all dilutions (Cheng et al., 2004). The results from the HR ICP-MS were replicated for a subset of groundwater samples with a precision of <5%. The accuracy and precision of the measurements were within ±10% when compared to known laboratory standards. The anions Br^-, Cl^-, F^- and SO_4^{2-} were analyzed using a Dionex Integrion HPIC System (Dionex, Thermo Scientific) with an AS-18 column, which has detection limits of 0.05 ppm and a precision of ±5% at typical concentrations. Sulfide concentrations were not measured but were generally low based on the correspondence between total S by ICPMS and sulfate measured by IC. DOC and DIC concentrations were analyzed for input solutions with a Shimadzu Carbon Analyzer with ±5% precision at Lamont-Doherty Earth Observatory.

2.6. Column transport parameterization

The Darcy velocity was calculated by dividing the average volume of samples by the cross-sectional area of columns (2 cm^2) and average sampling interval and ranged from 0.5 to 3 cm/h. The average bulk density ρ (ranged between 1.7 and 1.9 g/cm^3) of the columns was determined from oven dried sediment weight divided by the volume of dry sediment column (Table 1). The porosity θ (ranged between 0.29 and 0.34) was then estimated as: θ = 1- ρ/2.65, assuming a particle density of 2.65 g/cm^3. The dispersion coefficient (D) was determined (1.5 and 3 cm^2/h for slow and fast PWV, respectively) by fitting the bromide (Br^-) breakthrough curve using the analytical solution for one-dimensional advection-dispersion equation assuming conservative transport of Br^- (i.e. a retardation factor of 1) in the sand columns (Fig. S3).

2.7. Model formulation

We used a single-phase as well as a two-phase reversible non-linear kinetic model (Selim, 2014) to predict the observed As breakthrough, after modifying it to accommodate an initial exchangeable pool of As. The central scenario is based on the two-phase model. Because the retention and release of solute was time-dependent under the experimental conditions, kinetic reactions were employed instead of a local equilibrium assumption.

We used the one dimensional advection-dispersion equation to formulate the transport of arsenic in the sediment columns (Lapidus and Amundson, 1952):

$$\theta\frac{\partial C}{\partial t}+\rho\frac{\partial S}{\partial t}=\theta D\frac{\partial^2 C}{\partial^2 x}-v\frac{\partial C}{\partial x} \quad (1)$$

where, θ indicates the porosity of sand columns (dimensionless), ρ is the sediment bulk density (g/cm^3), C represents solute concentration (mg/L), S indicates the total sorbed concentration (mg/kg), D is the hydrodynamic dispersion coefficient (cm^2/hour), v represents the PWV (cm/hour), which is Darcy's velocity divided by θ and x is the length of column (cm) (Table 1) .

The equations for a two-phase reversible non-linear kinetic model with adsorption (forward) and desorption (reverse) rate constants are:

$$\rho\frac{\partial S_1}{\partial t}=\theta k_1 C^n-\rho k_2 S_1 \quad (2)$$

$$\rho\frac{\partial S_2}{\partial t}=\theta k_3 C^n-\rho k_4 S_2 \quad (3)$$

$$S=S_1+S_2 \quad (4)$$

where, the parameters k_1 and k_3 are the forward rate constant (hr^{-1}), k_2 and k_4 are the reverse rate constants (hr^{-1}), and n is the reaction order which is also a measure of variability in sorption sites in terms of arsenic retention (Zhang and Selim, 2005; Selim, 2014). The sorbed phase S_1 is assumed to react rapidly with the dissolved concentration C whereas sorbed phase S_2 is assumed to react slowly with C. The single-phase model assumes $S_2 = 0$ mg/kg. The numerical transport models were simulated using a Gaussian elimination method (Carnahan et al., 1969; Selim, 2014).

The two-phase model assumes: (a) any initial release of As is due to desorption from an initial, rapidly exchanged pool of sorbed As; (b) the pool of total sorbed As (S) in the sediment is comprised of two components: the first phase (S_1) is the fast reacting phosphate extractable As and the second phase (S_2) is a slow reacting phase, which is the difference between the bulk sediment As concentration (S) and S_1. The adsorbed pools of As in S_1 and S_2 are estimated based on total As and laboratory phosphate extractions (Table 2). For a single solid phase, the initial sorbed concentrations were adjusted while keeping the same k_1 and k_2 (associated with S_1) used in the two-phase model (Table S1).

3. Results

3.1. Sediment properties

Bulk As concentrations measured by XRF in the gray Holocene sediment ranged between 1 and 4 mg/kg (n = 7) (Table 2). Bulk As concentrations in the Pleistocene orange sediment ranged from 1.8 to 3.0 mg/kg (n = 7). In gray sand, iron (Fe) and calcium (Ca) concentrations averaged 1.5% and 6.9 g/kg, respectively. Overall, the orange sediment contained a higher concentration of Fe (2.5%) and a lower concentration of Ca (4.4 g/kg) than gray sediment.

The difference in reflectance (ΔR = 530 nm−520 nm) averaged 0.22 (n = 11) for gray sands, which corresponds to about 80% Fe(II) in the hot-acid leachable fraction of Fe(II + III) oxides in the sediment. The ΔR for the orange sands averaged 1.1 (n = 10), which indicates the absence of detectable Fe(II) in the fraction of hot-acid leachable Fe oxides.

The average proportions of Fe(II) measured by XAS analysis in freshly collected gray and orange sediments were 82 ± 6% and 8 ± 3% (n = 2), respectively. The most abundant Fe mineral classes in the gray sediment were Fe silicates (20 ± 3% biotite and 57 ± 4% Fe(II/III) silicates), with small and variable proportion of goethite, siderite, and little if any reactive Fe oxides (Table 3). In contrast, the orange sediments were primarily composed of reactive Fe oxides (65 ± 6%), and small quantities of goethite, nontronite and Fe(II/III) silicates.

Phosphate extractations were used to differentiate labile and nonlabile As pools. The gray sediment contains an average of about 3 mg/kg of total As, and about half (50%) of that is P-extractable (Table 2). The orange sediment also contains an average of about 2 mg/kg of As, but only about 15% is P-extractable. Therefore, on an average, the gray sediment contains five times more P-extractable As than orange sediment.

Table 3
Linear combination fitting results (%) of Fe EXAFS spectra for pristine orange and gray sediment cores.

Core depth	goethite	nontronite	Fe(II/III) silicates	hematite	ferrihydrite	pyrite	biotite	siderite	hornblende	magnetite
Pleistocene orange sediments										
13.5 m	–	20.4 ± 4.6	–	–	65.6 ± 2.4	1.3 ± 0.9	–	7.4 ± 1.7	–	–
15 m	12.8 ± 0	–	6.5 ± 4.3	–	63.8 ± 8.9	–	–	–	–	–
Holocene gray sediments										
12.8 m	–	–	44.8 ± 5.1	–	–	2.5 ± 1.7	26.7 ± 4.1	6.2 ± 3.6	–	–
15.5 m	17 ± 0	–	69.1 ± 2.7	–	–	–	13.9 ± 2.3	–	–	–

Note: Linear combination fittings were performed using five reference compounds, which means '-' in the table does not necessarily indicate that the mineral is absent in the column sample. Augite is the spectral component used as representative of Fe(II/III) silicates.

3.2. Influent groundwater composition

The source groundwater selected to elute the sediment columns was consistently high in dissolved As (320 ± 11 μg/L) and Fe (7 ± 0.4 mg/L) over the course of the experiment (Fig. S2a-b and e). The water contained moderately high levels of manganese (3 mg/L Mn), phosphate (1.5 mg/L as P), sulfate (3 mg/L as SO_4–S), and bicarbonate (104 mg/L as DIC) (Figs. S1e-g and S2c-d, f). There was no detectable dissolved oxygen in the groundwater (DO kit reading of 0 ppb), the ORP readings remained negative (−105 to −134 mV), and the pH was consistent at 7.0 ± 0.1 throughout the experimental period (Fig. S2i-j). The composition of groundwater remained unaltered in the overflowing storage bag. Arsenic was present mainly as As(III) (>90%) in groundwater collected from the well and the storage bag (n = 8 each) (Fig S2e). The dissolved organic carbon (DOC) concentration in the input groundwater was about 3 mg/L.

3.3. Initial effluent data for As and other redox-sensitive parameters

3.3.1. Pleistocene orange sediment columns

Concentrations of As remained below 10 μg/L in the effluent for about 40 pore volumes (PV) in the two orange sand columns eluted at a pore water velocity (PWV) of about 80 cm/day (Fig. 3b), but only for 10 PV at PWVs of 156 cm/day and 40 cm/day (Fig. 3a and c). Initial breakthrough of As (50% of the input concentration of 320 μg/L) was observed after about 50 PV at a PWV of 156 cm/day and after 70 PV in a column with a PWV of 80 cm/day. Breakthrough of As did not quite reach 50% in the 40 cm/day PWV column. In all columns, Fe concentrations in the effluent remained below 1 mg/L despite a high input of 7 mg/L of Fe (Fig. 3d–f). In contrast, S levels in the effluent started immediately about 20% above the influent concentration of 3 mg/L and dropped to 50% of the input (1.5 mg/L) after about 100 PV at 156 cm/day PWV, after 70 PV at 80 cm/day

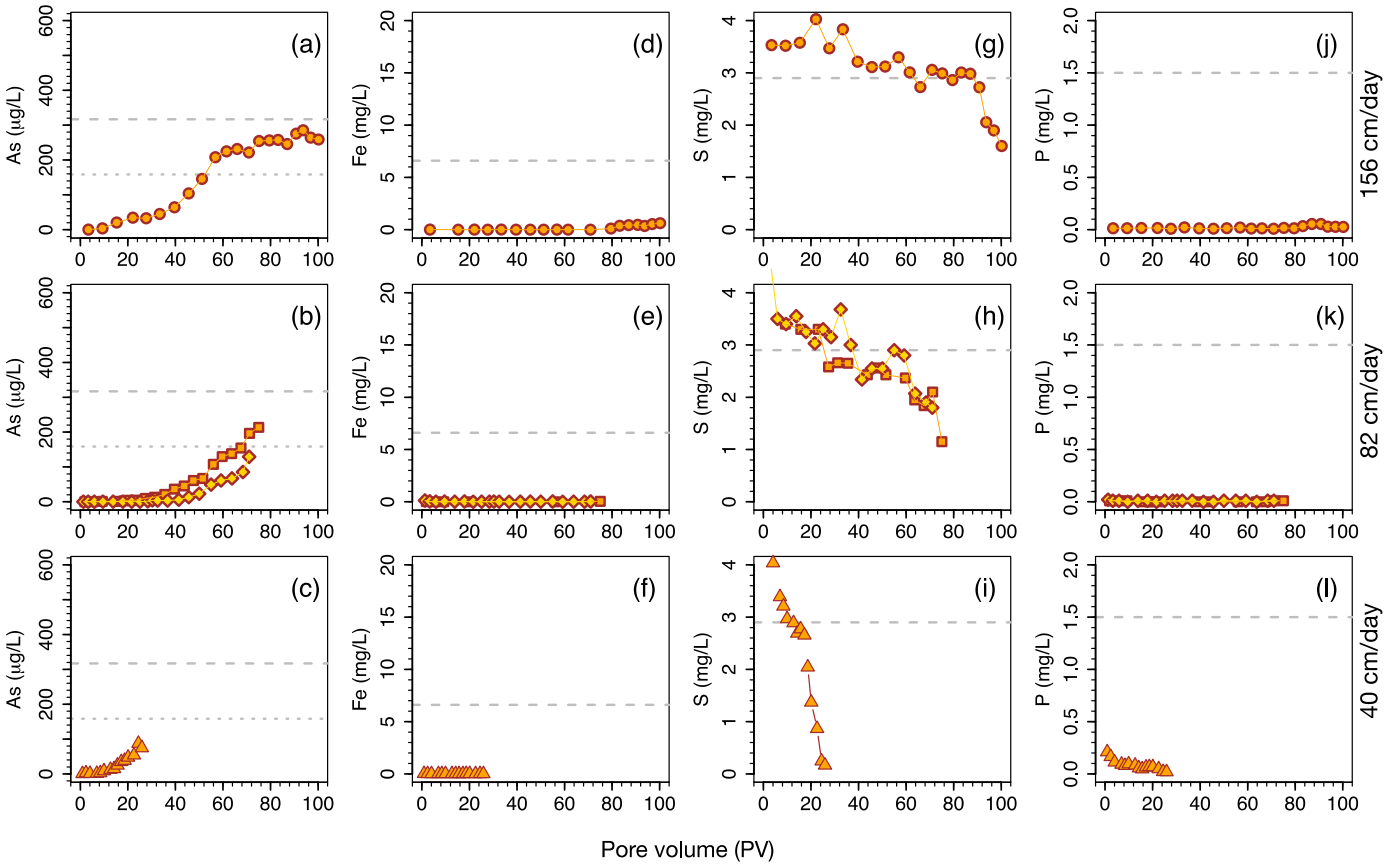

Fig. 3. Arsenic (a–c), iron (d–f), sulfur (g–i), and phosphorus (j–l) in the effluent of orange Pleistocene sediment columns. Arsenic and other redox-sensitive parameters plotted as a function of pore volume at a pore-water velocity (PWV) of 156 cm/day (top panels, n = 1), 81.6 cm/day (middle panels, n = 2), and 40 cm/day (bottom panels, n = 1). Input groundwater concentrations of each analyte are indicated by the gray dashed line in each plot. The gray dotted line (a-c) indicates 50% of the input As concentration. The same vertical axes of Fig. 4 are maintained for the ease of comparison.

PWV, and after only 20 PV at a PWV of 40 cm/day (Fig. 3g–i). The inflow contained 1.5 mg/L P, most of which was retained in orange sand columns for the entire experiment (Fig. 3j-l).

3.3.2. Holocene gray sediment columns

Concentrations of As in the first 50 PV of effluent from the gray columns were consistently higher than for the orange columns and varied between 10 and 200 μg/L (Fig. 4a–c). For the 4 fast flow columns at a PWV of 150–230 cm/day, As concentrations gradually increased to reach the inflow concentration of 320 μg/L at about 60–70 PV and up to about 500 μg/L at about 80 PV (Fig. 4a and c). For 1 out of the 2 slow-flow gray sand columns eluted at a PWV of 72 cm/day, effluent As concentrations reached the influent level at about 40 PV, while both slow-flow columns reached the initial breakthrough at about 30 PV (Fig. 4b). In contrast to the orange columns, concentrations of Fe in the effluent reached inflow concentration of 7 mg/L after 70 and 30 PV in the fast- and slow-flow columns of gray sand, respectively (Fig. 4d–e). About 10–20 PV later, concentration of Fe in effluent from the gray sediment columns reached 15–20 mg/L. As in the case of the orange sand columns, concentrations of S in effluent from the gray sand columns started immediately at 3.5 mg/L, somewhat higher than the inflow, and dropped below 50% of the input after 70 PV and at 30 PV for the fast- and slow-flow columns of gray sand, respectively (Fig. 4g and h). Unlike the orange sediment columns, concentrations of P in effluent from the gray sediment columns gradually rose for both the fast-flow and the slow-flow columns (Fig. 4j-l).

3.3.3. Pure sand column

Arsenic and iron concentrations in effluent from the pure sand column reached levels of the inflow within about 10 PV and then showed fluctuations around an average that is slightly below that of the input (Fig. 5a and b). Concentration of P in the effluent took about 60 PV to reach about two-thirds of the inflow concentration (Fig. 5d). As in the case of orange and gray columns (Figs. 3g–i and 4g-i), concentrations of S started a little above concentration in the inflow and then declined steadily to <0.5 mg/L at about 100 PV (Fig. 5c).

3.4. Effluent data from the later phase of the experiment

The later phases of the experiment were affected by the redox chemistry of Fe and S, in most cases well after As breakthrough (Figs. S4 and S5). The changes in Fe and S concentrations during the experiments were distinct from the breakthrough curves and showed both transient pulses in Fe and a rapid decline in effluent S concentrations (Figs. S4d-i and S5d-i). Iron concentrations were generally low and only increased above 1 mg/L after about 150 PV in the orange sand columns (Fig. S4d and e). Sulfur concentrations in the effluent dropped to <0.5 mg/L in both orange and gray sediment columns, primarily after the initial breakthrough of As took place. Following the precipitous drop, S in the effluent briefly rose above 0.5 mg/L in the orange sand columns, but only after 150 PV at 156 or 80 PWV and after 50 PV at 80 PWV (Fig. S4g–i). The later effluent data also showed multiple breakthroughs of As in both gray and orange sand columns (Figs. S4a–b and S5a-b). The

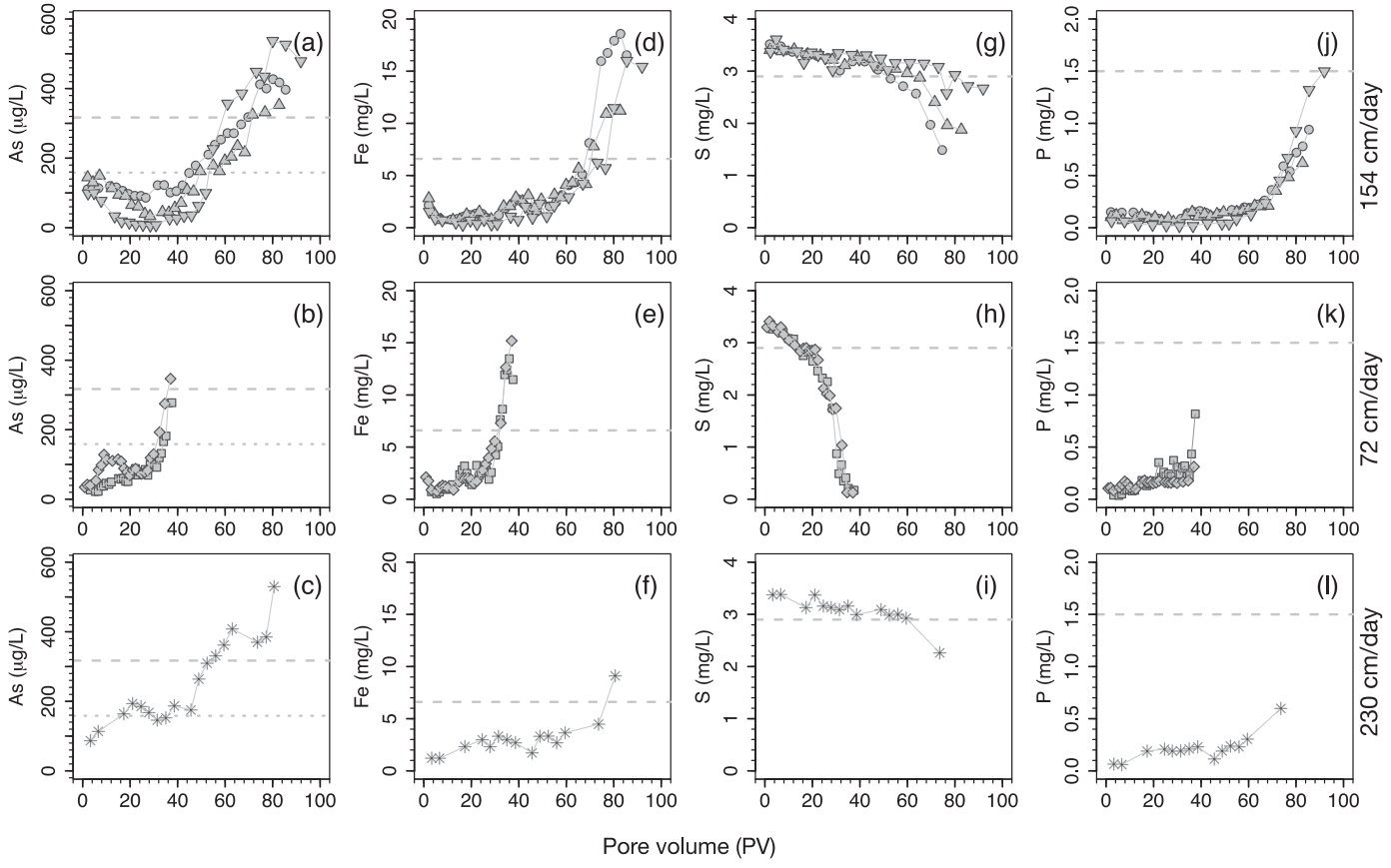

Fig. 4. Arsenic (a–c), iron (d–f), sulfur (g–i), and phosphorus (j–l) in the effluent of gray Holocene sediment columns. Arsenic and other redox-sensitive parameters plotted as a function of pore volume at a PWV of 154 cm/day (top panels, n = 3), 72 cm/day (middle panels, n = 2), and 230 cm/day (bottom panels, n = 1). Input groundwater concentrations of each analyte are indicated by the gray dashed line in each plot. The gray dotted line (a-c) indicates 50% of the input As concentration. The PWV of the top two panels are comparable to that of Fig. 3.

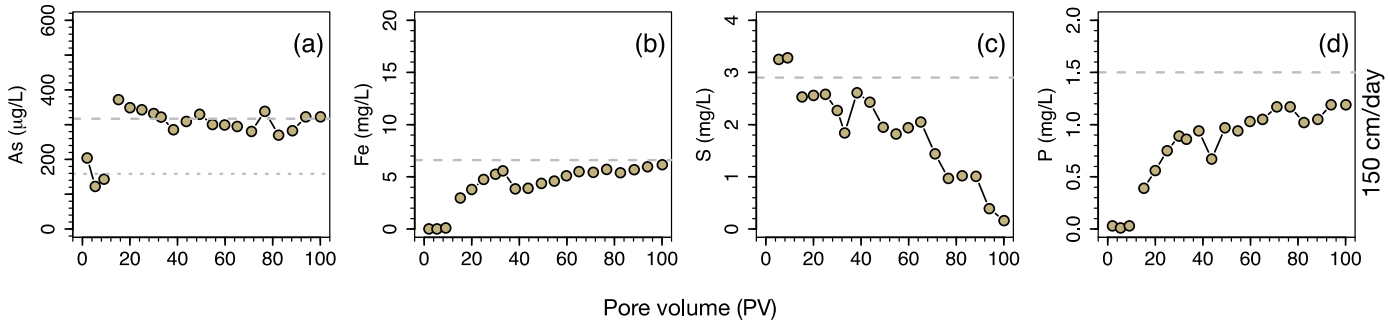

Fig. 5. Concentrations of arsenic (a), iron (b), sulfur (c) and phosphorus (d) in the pure sand column plotted as a function of pore volume. Input groundwater concentrations of each analyte are indicated by the gray dashed line in each plot. The gray dotted line (a-c) indicates 50% of the input As concentration.

present study focuses on the early As breakthrough rather than the subsequent changes in effluent chemistry.

4. Discussion

4.1. Transport of arsenic and other redox-sensitive parameters

Typical breakthrough curves for reactive (non-conservative) ion transport through sediments typically show strong retention until the mineral phases are saturated with ions, and then rapid and complete breakthrough (Selim, 2014). Arsenic transport in the present experiments was more complex, with early and partial breakthrough, and effluent As levels that did not stabilize (Figs. 3a–c and 4a-c). Despite these differences, several common features were observed in most columns.

There are multiple pools of As in gray and orange sands, and desorption from the more weakly retained pool by phosphate appears to enhance elution. In gray columns, in which about half of As was found in this phosphate-extractable pool (Table 2), the data suggest that this As pool is efficiently released into the effluent from the onset of the experiment (Fig. 4a–c). There was also a short-lived pulse of As released into solution when four-times higher than the input phosphate level was added to groundwater (Figs. S2d and S7), suggesting the rise of effluent As beyond the input level could also be attributed to competitive desorption by phosphate. The mechanism can also be described as a "snow-plough effect" where an incoming solution with a high solute concentration displaces resident cations from the exchange sites (Barry et al., 1983).

In orange sediments, the labile pool is much smaller and As is to a large extent retained during the early stages of transport (Fig. 3a–c). The breakthrough of As after the initial release phase in the gray sediment columns is more rapid than that in orange sediment columns, indicating a pool of As in orange sand becomes irreversibly adsorbed over time. A rapid early rise in As concentrations followed by a slower approach to equilibrium is consistent with previous experiments conducted with orange sand (Radloff et al., 2011). A possible alternative explanation is that gray sediments may have less effectively sorbed As than orange sediments under the experimental conditions.

In most of the columns, the initial breakthrough of As occurred within 30–70 PV, depending on the flow rate (Figs. 3a–b and 4a–c). The differences in As breakthrough as a function of PWV indicates that adsorption is kinetically limited under the range of experimental conditions (Darland and Inskeep, 1997). Due to kinetic limitation, the breakthrough of As takes place earlier at fast PWV as a function of time, while slower flow allows for increased reaction times, increased adsorption, and delayed (or partial) breakthrough. Given kinetic limitation, As transport is more consistent between columns when plotted as a function of time rather than pore volume (Fig. 6). Kinetic limitation was also reflected in other redox-sensitive parameters. Sulfur, in particular, was consumed in the effluent earlier at slower PWV (Figs. 3g–i and 4g-i), but at around the same time when plotted as a function of time.

The initial effluent data show that As transport was affected primarily by adsorption and desorption, which is consistent with the conclusion of previous studies (e.g. Stollenwerk et al., 2007). Changes in Fe and S redox status were observed mostly during the later phases of the experiment, when they affected both As speciation and Fe mineralogy (Figs. S4 and S5). The delay in redox transformation can be attributed to lag phase microbial growth, which is widespread and occurs during the time microbes adapt to changing groundwater conditions. For example, a metabolic time lag of up to 20 days was observed between acetate addition and the onset of S-reduction at the Uranium Mill Tailings Site in Colorado (Druhan et al., 2012), indicating prolonged suppression of S-reducing bacterial activity. Similarly, experimental data in our columns indicate a significant lag-time of about 100–120 h in the build-up of S-reducing bacteria prior to the onset of any noticeable S-reduction. We conclude that S-reduction affected the transport properties of As sorption only after S was removed from column effluents.

The extent of Fe reduction in these columns was evidently limited by the availability of reactive DOC. Assuming 1 mol of DOC is required to reduce 4 mol of Fe(III) to 4 mol of Fe(II) (Postma et al., 2007), 3 mg/L of entirely reactive DOC supplied could have reduced 80% of the entire volume of the orange sand to gray after three weeks of flow period based on a simple stoichiometric calculation (Mihajlov et al., 2020; Mozumder et al., 2020). Visual inspection of sediment color, however, did not reveal such a dramatic change in the redox state of Fe, suggesting little As was released due Fe reductive compared to the high concentration of 320 µg/L As in the inflow water.

Unlike As, both Fe and P were more effectively sequestered onto the orange sand than in gray sand (Figs. 3d–f, j-l and 4d–f, j-l). The average bulk Fe content in the orange sediment columns (2.4%) is about 1% higher than that in gray sand columns (1.5%). The proportion of Fe(III) in orange sand is almost one order of magnitude higher than that in gray sand. The data suggest sequestration of P and Fe(II) was enhanced in orange sands containing a higher proportion of Fe(III) minerals.

4.2. Modeling arsenic transport

A direct comparison of As transport in gray and orange sediments is possible by comparing the early stage elution of As from columns. Adsorption and desorption of As was the predominant

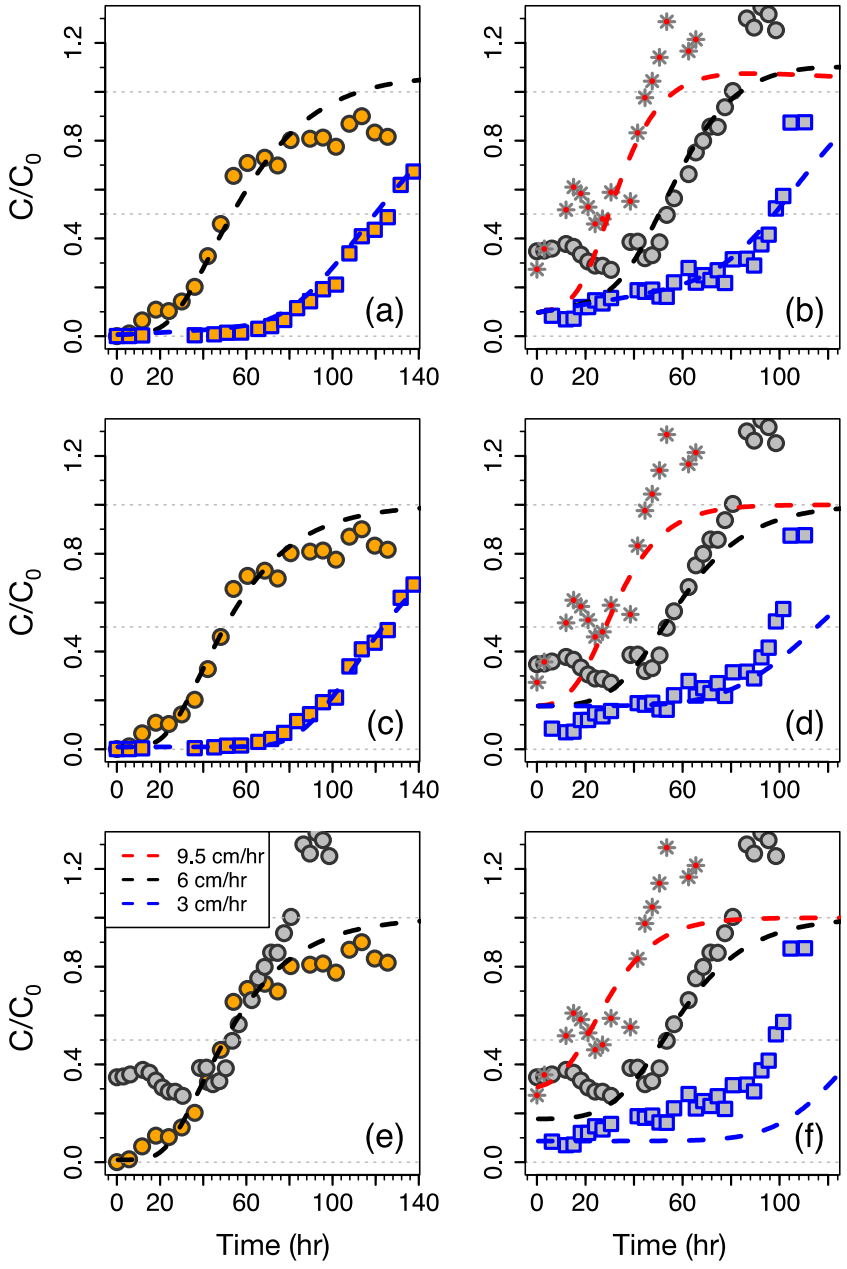

Fig. 6. Modeled effluent As over time. Concentrations of As in the effluent (C) relative to the inflow concentration (C_0) for the six scenarios listed in Table S1 are shown by dashed lines color-coded according to three PWV (Table 1). (a) 2-phase model for orange sands, (b) 2-phase model for gray sands, (c) single-phase model for orange sands, (d) single-phase model for gray sands, (e) single-phase model with the same rate constants used for orange and gray sands, and (e) single-phase model for gray sands at different initial solid phase As concentrations.

process during this interval, and As breakthrough was observed in many columns (Figs. 3a–b and 4a-c). Later in the experiment, redox transformations became more important and likely affected As partitioning. It is difficult to separate adsorption-desorption processes from redox processes using a simple model. For this reason, our modeling effort is focused here on the first 3–5 days of As data that were largely unaffected by redox-processes.

In order to simulate the observations, an average input As concentration of 320 μg/L, porosity of 0.32, bulk density of 1.80 g/cm^3, and a reaction order of 0.4 (a fitting parameter) were used. The variable transport parameters were the measured flow velocities, corresponding dispersion coefficient, initial sorbed phase As concentrations, and associated forward (k_1, k_3) and reverse (k_2, k_4) rate constants. For the two-phase fully reversible kinetic model, the initial sorbed phases, S_1 and S_2 for the gray sand were 1.5 and 1.5 mg/kg (S = 3 mg/kg), respectively, whereas for the orange sand they were 0.3 and 1.7 mg/kg (S = 2 mg/kg), respectively (Table S1). The adjusted initial sorbed As concentration for the single-phase kinetic model were 2 and 0.5 mg/kg for the gray and orange sediment columns, respectively.

For the two-phase transport model, one single set of rate constants was used for all gray sediment columns and another single set for all orange sediment columns, irrespective of PWV (Fig. 6a and b). The forward and reverse rate constants determined for the

gray sediment columns associated with S_1 are 6 h^{-1} (k_1) and 0.17 h^{-1} (k_2), and for S_2 are 0.01 h^{-1} (k_3) and 0.008 h^{-1} (k_4), respectively. The two-phase model reproduced effluent concentrations with an initial release (starting at $C/C_0 = 0.1$) as well as exceedance ($C/C_0 = 1.1$) above the influent level in gray sediments. A single solid phase model ($k_1 = 6$ h^{-1} and $k_2 = 0.17$ h^{-1}) can also predict As breakthrough with an initial release, but fails to reproduce a higher concentration than that in the inflow; i.e. $C/C_0 > 1$ (Fig. 6d). The initial release of As is a function of the amount of weakly retained pool of sorbed As that is susceptible to desorption (Fig. 6f).

With the two-phase model, the forward and reverse rate constants determined for the orange sand columns for S_1 are 2 h^{-1} (k_1) and 0.057 h^{-1} (k_2) and for S_2 are 0.01 h^{-1} (k_3) and 0.008 h^{-1} (k_4) (Fig. 6a). The rate constants associated with the fast reacting phase (S_1) are three fold smaller than that in gray sand. The rates associated with the slow reacting phase (S_2) are the same derived for gray sand ($k_3 = 0.01$ h^{-1} and $k_4 = 0.008$ h^{-1}). Because S_1 is 5 times smaller than that in gray sand (0.3 compared to 1.5 mg/kg), the initial release of As is insignificant (Fig. 6a and c). A single-phase model ($k_1 = 2$ h^{-1} and $k_2 = 0.07$ h^{-1}) can also be used to adequately describe the breakthrough of As in orange sediment columns (Fig. 6c).

Due to a higher fraction of weakly bound As in the gray sand columns, larger rate constants were needed to predict As breakthrough. If we ignore the initial As release and overshoot ($C/C_0 > 1$) portion of the effluent data and focus on the main breakthrough, the same set of rate constants used for orange sand ($k_1 = 2$ h^{-1} and $k_2 = 0.07$ h^{-1}) could also be applied for gray sand (e.g. Fig. 6e). The shallow groundwater is generally low in P in the area and ideally will not desorb As at the rate we observed in these experimental columns. The smaller set of rate constants are comparable to the sorption and desorption coefficients determined for arsenite in earlier studies (Elkhatib et al., 1984a, b; Barrachina et al., 1996).

4.3. Retardation of arsenic

The apparent retention of As in the experimental columns can be determined from the ratio of forward and reverse rate constants ($k_1/k_2 \approx 30$ to 35). The As retention factor or retardation factor is the ratio of the adsorbed pool that is retained within the solid matrix to the much smaller desorbed pool that goes into the solution. The transport of As in Bangladesh groundwater, therefore, appears to be retarded by a factor of 30–35 relative to the flow of groundwater by both gray and orange sediments. This is surprising but not inconsistent with recent findings from batch adsorption experiments conducted under carefully controlled conditions (Thi Hoa Mai et al., 2014).

A retardation factor (R_f) of 30–35 corresponds to a K_D of about 5–6 L/kg according to the following equations, assuming a sediment bulk density of 1.8 g/cm^3 and porosity of 0.32:

$$R_f = 1 + \frac{\rho}{\theta} K_D \tag{5}$$

$$K_D = \frac{\theta \times \left(R_f - 1\right)}{\rho} \tag{6}$$

The estimated K_D of about 5–6 L/kg is similar to low-range partition coefficients determined with batch equilibrium experiments for Holocene gray sediments in Bangladesh (van Geen et al., 2008) and mid-range estimates from field observations for Pleistocene sands that were reduced over time in West Bengal, India (McArthur et al., 2008, 2011) and near Hanoi in Vietnam (van Geen et al., 2013).

4.4. Vulnerability of low-arsenic aquifers to pumping

An earlier As breakthrough at accelerated flow rates in the experimental columns (Fig. 6) suggest sedimentary aquifers of Bangladesh that are perturbed by pumping are more vulnerable to As contamination, irrespective of the redox status and age of aquifer sediment. Irrigation pumping for growing rice largely impacts the shallow groundwater flow system of Bangladesh (Harvey et al., 2002; van Geen et al., 2008) whereas municipal pumping has significantly altered the deeper flow-systems over the past two decades (Michael and Voss, 2008; Knappett et al., 2016; Khan et al., 2016; Mozumder et al., 2020; Mihajlov et al., 2020). These perturbations are likely to reduce As retardation over time and accelerate the spread of As in adversely As-affected rural areas.

At our study site in Araihazar, Bangladesh, a groundwater flow model constrained with hydraulic head measurements has shown that shallow groundwater (<30 m) can penetrate the intermediate (>40–90 m) low-As aquifers within 7–83 years after recharge (Mozumder et al., 2020). The simulations are consistent with the age of groundwater (11–69 years) measured at 14 monitoring wells, screened between 50 and 70 m, on the basis of tritium/helium ($^3H/^3He$) dating technique (Stute et al., 2007). No systematic correlation between high (low) As and detectable (undetectable) ^3H in the intermediate aquifer indicated instead a different source of As than that from the shallow aquifer. Assuming shallow groundwater As is retarded by a factor of 30, as determined in the present study, the intermediate wells are protected against the downward migration of As in the area for ~1000 years (average groundwater age of 35 years multiplied by 30). This is important because over the past decade, the number of privately installed intermediate wells' tapping the low-As Pleistocene aquifer has quadrupled in the study area and probably elsewhere in Bangladesh (Mozumder et al., 2020).

If adsorption provides significant protection against the downward migration of As, deep wells that are low in As (<10 μg/L) today will remain low in As for many decades. Indeed, more than a decade (2002–2015) of monitoring of a dozen deep community wells (CW-2, 5, 7, 34, 36, 41–43, 45–48) installed between 90 and 170 m in Araihazar indicates stable groundwater As concentrations of <1 to <10 μg/L. This appears to be the case in South-Central Bangladesh where 13 years of continuous monitoring data in a total of 46 deep wells (>150 m deep) revealed a relatively stable groundwater composition (Ravenscroft et al., 2013).

The results do not mean As concentrations in deep aquifers of Bangladesh will remain low everywhere. Nine out of 927 deep wells (>90 m deep) tested during a blanket survey in 2012–13 in the study area were elevated (>50 μg/L) in As (van Geen et al., 2014; Choudhury et al., 2016). Intermediate aquifers affected by pumping appear to be especially vulnerable to As contamination and should therefore be monitored more frequently (Mihajlov et al., 2020; Mozumder et al., 2020).

5. Conclusions

- Field-based column experiments require some effort to set up but allowed us to study the reactive transport of As through sediment with fewer perturbations than most previous experiments.
- During the initial period, As transport in the experimental columns was primarily controlled by adsorption and desorption, allowing us to determine a set of rate constants using a multi-reaction transport model. The estimated apparent K_D of ~5–6 L/kg suggests significant protection of low-As deep aquifers against the intrusion of shallow high As groundwater.

- Apparently because of a delay in microbial responses, the reduction of S and Fe became important only during the later phases of the experiment.

Declaration of competing interest

The authors declare that they have no known competing financial interests or personal relationships that could have appeared to influence the work reported in this paper.

Acknowledgement

This study was financially supported by U.S. National Institute of Environmental Health Sciences (grants ES010349 and ES009089) and NSF grant 1521356. Synchrotron based EXAFS analysis was conducted at the Stanford Synchrotron Radiation Lightsource (SSRL), a national user facility operated by Stanford University for the U.S. Department of Energy. Use of the Stanford Synchrotron Radiation Lightsource, SLAC National Accelerator Laboratory, is supported by the U.S. Department of Energy, Office of Science, Office of Basic Energy Sciences under Contract No. DE-AC02-76SF00515. We are thankful to Lamont technicians Tom Protus and Ryan Harris for providing mechanical support to construct custom-made equipment for the field experiment. We would also like to thank the two anonymous reviewers for their comments that greatly imporved the final manuscript. This is Lamont-Doherty Earth Observatory contribution number 8419.

Appendix A. Supplementary data

Supplementary data to this article can be found online at https://doi.org/10.1016/j.watres.2020.116081.

References

Ahmed, K.M., Bhattacharya, P., Hasan, M.A., Akhter, S.H., Alam, S.M.M., Bhuyian, M.A.H., Imam, M.B., Khan, A.A., Sracek, O., 2004. Arsenic enrichment in groundwater of the alluvial aquifers in Bangladesh: an overview. Applied Geochemistry, Arsenic in Groundwater of Sedimentary Aquifers 19, 181–200. https://doi.org/10.1016/j.apgeochem.2003.09.006.

Baes, C.F., Sharp, R.D., 1983. A proposal for estimation of soil leaching and leaching constants for use in assessment models. J. Environ. Qual. 12, 17–28. https://doi.org/10.2134/jeq1983.00472425001200010003x.

Barrachina, A.C., Carbonell, F.B., Beneyto, J.M., 1996. Kinetics of arsenite sorption and desorption in Spanish soils. Commun. Soil Sci. Plant Anal. 27, 3101–3117. https://doi.org/10.1080/00103629609369764.

Barry, D.A., Starr, J.L., Parlange, J.-Y., Braddock, R.D., 1983. Numerical analysis of the snow-plow effect. Soil Sci. Soc. Am. J. 47, 862–868. https://doi.org/10.2136/sssaj1983.03615995004700050004x.

Berg, M., Tran, H.C., Nguyen, T.C., Pham, H.V., Schertenleib, R., Giger, W., 2001. Arsenic contamination of groundwater and drinking water in Vietnam: A human Health threat. Environ. Sci. Technol. 35, 2621–2626. https://doi.org/10.1021/es010027y.

Bhattacharya, P., Chatterjee, D., Jacks, G., 1997. Occurrence of arsenic-contaminated groundwater in alluvial aquifers from Delta plains, eastern India: options for safe drinking water supply. Int. J. Water Resour. Dev. 13, 79–92. https://doi.org/10.1080/07900629749944.

Carnahan, B., Luther, H.A., Wilkes, J.O., 1969. Applied Numerical Methods. Wiley, New York.

Cheng, Z., Zheng, Y., Mortlock, R., Geen, A. van, 2004. Rapid multi-element analysis of groundwater by high-resolution inductively coupled plasma mass spectrometry. Anal. Bioanal. Chem. 379, 512–518. https://doi.org/10.1007/s00216-004-2618-x.

Choudhury, I., Ahmed, K.M., Hasan, M., Mozumder, M.R.H., Knappett, P.S.K., Ellis, T., van Geen, A., 2016. Evidence for elevated levels of arsenic in public wells of Bangladesh due to improper installation. Ground Water 54, 871–877. https://doi.org/10.1111/gwat.12417.

Darland, J.E., Inskeep, W.P., 1997. Effects of pore water velocity on the transport of arsenate. Environ. Sci. Technol. 31, 704–709. https://doi.org/10.1021/es960247p.

Dixit, S., Hering, J.G., 2003. Comparison of arsenic(V) and arsenic(III) sorption onto iron oxide minerals: implications for arsenic mobility. Environ. Sci. Technol. 37, 4182–4189. https://doi.org/10.1021/es030309t.

DPHE/BGS, 2001. Arsenic Contamination of Groundwater in Bangladesh. BGS, Keyworth.

Druhan, J.L., Steefel, C.I., Molins, S., Williams, K.H., Conrad, M.E., DePaolo, D.J., 2012. Timing the onset of sulfate reduction over multiple subsurface acetate amendments by measurement and modeling of sulfur isotope fractionation. Environ. Sci. Technol. 46, 8895–8902. https://doi.org/10.1021/es302016p.

Elkhatib, E.A., Bennett, O.L., Wright, R.J., 1984a. Arsenite sorption and desorption in soils. Soil Sci. Soc. Am. J. 48, 1025–1030. https://doi.org/10.2136/sssaj1984.03615995004800050015x.

Elkhatib, E.A., Bennett, O.L., Wright, R.J., 1984b. Kinetics of arsenite sorption in soils. Soil Sci. Soc. Am. J. 48, 758–762. https://doi.org/10.2136/sssaj1984.03615995004800040012x.

Fendorf, S., Michael, H.A., Geen, A. van, 2010. Spatial and temporal variations of groundwater arsenic in South and Southeast Asia. Science 328, 1123–1127. https://doi.org/10.1126/science.1172974.

Harvey, C.F., Swartz, C.H., Badruzzaman, A.B., Keon-Blute, N., Yu, W., Ali, M.A., Jay, J., Beckie, R., Niedan, V., Brabander, D., Oates, P.M., Ashfaque, K.N., Islam, S., Hemond, H.F., Ahmed, M.F., 2002. Arsenic mobility and groundwater extraction in Bangladesh. Science 298, 1602–1606. https://doi.org/10.1126/science.1076978.

Horneman, A., Van Geen, A., Kent, D.V., Mathe, P.E., Zheng, Y., Dhar, R.K., O'Connell, S., Hoque, M.A., Aziz, Z., Shamsudduha, M., Seddique, A.A., Ahmed, K.M., 2004. Decoupling of as and Fe release to Bangladesh groundwater under reducing conditions. Part 1: Evidence from sediment profiles. Geochem. Cosmochim. Acta 68, 3459–3473. https://doi.org/10.1016/J.Gca.2004.01.026.

Itai, T., Takahashi, Y., Seddique, A.A., Maruoka, T., Mitamura, M., 2010. Variations in the redox state of as and Fe measured by X-ray absorption spectroscopy in aquifers of Bangladesh and their effect on as adsorption. Appl. Geochem. 25, 34–47. https://doi.org/10.1016/j.apgeochem.2009.09.026.

Jung, H.B., Bostick, B.C., Zheng, Y., 2012. Field, experimental, and modeling study of arsenic partitioning across a redox transition in a Bangladesh aquifer. Environ. Sci. Technol. 46, 1388–1395. https://doi.org/10.1021/es2032967.

Khan, M.R., Koneshloo, M., Knappett, P.S.K., Ahmed, K.M., Bostick, B.C., Mailloux, B.J., Mozumder, R.H., Zahid, A., Harvey, C.F., van Geen, A., Michael, H.A., 2016. Megacity pumping and preferential flow threaten groundwater quality. Nat. Commun. 7, 12833. https://doi.org/10.1038/ncomms12833.

Knappett, P.S.K., Mailloux, B.J., Choudhury, I., Khan, M.R., Michael, H.A., Barua, S., Mondal, D.R., Steckler, M.S., Akhter, S.H., Ahmed, K.M., Bostick, B., Harvey, C.F., Shamsudduha, M., Shuai, P., Mihajlov, I., Mozumder, R., van Geen, A., 2016. Vulnerability of low-arsenic aquifers to municipal pumping in Bangladesh. J. Hydrol. 539, 674–686. https://doi.org/10.1016/j.jhydrol.2016.05.035.

Lapidus, L., Amundson, N.R., 1952. Mathematics of adsorption in beds. VI. The effect of longitudinal diffusion in ion exchange and chromatographic columns. J. Phys. Chem. 56, 984–988. https://doi.org/10.1021/j150500a014.

McArthur, J.M., Nath, B., Banerjee, D.M., Purohit, R., Grassineau, N., 2011. Palaeosol control on groundwater flow and pollutant distribution: the example of arsenic. Environ. Sci. Technol. 45, 1376–1383. https://doi.org/10.1021/es1032376.

McArthur, J.M., Ravenscroft, P., Banerjee, D.M., Milsom, J., Hudson-Edwards, K.A., Sengupta, S., Bristow, C., Sarkar, A., Tonkin, S., Purohit, R., 2008. How paleosols influence groundwater flow and arsenic pollution: a model from the Bengal Basin and its worldwide implication. Water Resour. Res. 44, W11411 https://doi.org/10.1029/2007WR006552.

Meng, X., Korfiatis, G.P., Jing, C., Christodoulatos, C., 2001. Redox transformations of arsenic and iron in water treatment sludge during aging and TCLP extraction. Environ. Sci. Technol. 35, 3476–3481. https://doi.org/10.1021/es010645e.

Michael, H.A., Voss, C.I., 2008. Evaluation of the sustainability of deep groundwater as an arsenic-safe resource in the Bengal Basin. Proc. Natl. Acad. Sci. Unit. States Am. https://doi.org/10.1073/pnas.0710477105.

Mihajlov, I., Mozumder, M.R.H., Bostick, B.C., Stute, M., Mailloux, B.J., Knappett, P.S.K., Choudhury, I., Ahmed, K.M., Schlosser, P., van Geen, A., 2020. Arsenic contamination of Bangladesh aquifers exacerbated by clay layers. Nat. Commun. 11, 2244. https://doi.org/10.1038/s41467-020-16104-z.

Mozumder, M.R.H., Michael, H.A., Mihajlov, I., Khan, M.R., Knappett, P.S.K., Bostick, B.C., Mailloux, B.J., Ahmed, K.M., Choudhury, I., Koffman, T., Ellis, T., Whaley-Martin, K., Pedro, R.S., Slater, G., Stute, M., Schlosser, P., Geen, A. van, 2020. Origin of groundwater arsenic in a rural Pleistocene aquifer in Bangladesh depressurized by distal municipal pumping. Water Resources Research n/a. https://doi.org/10.1029/2020WR027178 e2020WR027178.

Newville, M., 2001. IFEFFIT: interactive XAFS analysis and FEFF fitting. J. Synchrotron Radiat. 8, 322–324. https://doi.org/10.1107/s0909049500016964.

Nickson, R., McArthur, J., Burgess, W., Ahmed, K.M., Ravenscroft, P., Rahman, M., 1998. Arsenic poisoning of Bangladesh groundwater. Nature 395, 338. https://doi.org/10.1038/26387.

Postma, D., Larsen, F., Minh Hue, N.T., Duc, M.T., Viet, P.H., Nhan, P.Q., Jessen, S., 2007. Arsenic in groundwater of the Red River floodplain, Vietnam: controlling geochemical processes and reactive transport modeling. Geochem. Cosmochim. Acta 71, 5054–5071. https://doi.org/10.1016/j.gca.2007.08.020.

Radloff, K.A., Zheng, Y., Michael, H.A., Stute, M., Bostick, B.C., Mihajlov, I., Bounds, M., Huq, M.R., Choudhury, I., Rahman, M.W., Schlosser, P., Ahmed, K.M., van Geen, A., 2011. Arsenic migration to deep groundwater in Bangladesh influenced by adsorption and water demand. Nat. Geosci. 4, 793–798. https://doi.org/10.1038/ngeo1283.

Radloff, K.A., Zheng, Y., Stute, M., Weinman, B., Bostick, B., Mihajlov, I., Bounds, M., Rahman, M.M., Huq, M.R., Ahmed, K.M., Schlosser, P., van Geen, A., 2015. Reversible adsorption and flushing of arsenic in a shallow, Holocene aquifer of Bangladesh. Appl. Geochem. https://doi.org/10.1016/j.apgeochem.2015.11.003.

Ravenscroft, P., Brammer, H., Richards, K., 2009. Arsenic Pollution: a Global

Synthesis. Wiley-Blackwell.
Ravenscroft, P., McArthur, J.M., Hoque, M.A., 2013. Stable groundwater quality in deep aquifers of Southern Bangladesh: the case against sustainable abstraction. Sci. Total Environ. 454, 627–638. https://doi.org/10.1016/j.scitotenv.2013.02.071, 455.
Robinson, C., Brömssen, M. von, Bhattacharya, P., Häller, S., Bivén, A., Hossain, M., Jacks, G., Ahmed, K.M., Hasan, M.A., Thunvik, R., 2011. Dynamics of arsenic adsorption in the targeted arsenic-safe aquifers in Matlab, south-eastern Bangladesh: insight from experimental studies. Applied Geochemistry, Arsenic and other toxic elements in global groundwater systems 26, 624–635. https://doi.org/10.1016/j.apgeochem.2011.01.019.
Selim, H.M., 2014. Transport & Fate of Chemicals in Soils: Principles & Applications.
Shoenfelt, E.M., Winckler, G., Lamy, F., Anderson, R.F., Bostick, B.C., 2018. Highly bioavailable dust-borne iron delivered to the Southern Ocean during glacial periods. Proc. Natl. Acad. Sci. Unit. States Am., 201809755. https://doi.org/10.1073/pnas.1809755115.
Smedley, P.L., Kinniburgh, D.G., 2002. A review of the source, behaviour and distribution of arsenic in natural waters. Appl. Geochem. 17, 517–568. https://doi.org/10.1016/S0883-2927(02)00018-5.
Stollenwerk, K.G., Breit, G.N., Welch, A.H., Yount, J.C., Whitney, J.W., Foster, A.L., Uddin, M.N., Majumder, R.K., Ahmed, N., 2007. Arsenic attenuation by oxidized aquifer sediments in Bangladesh. Science of The Total Environment, Arsenic in the Environment: Biology and Chemistry 379, 133–150. https://doi.org/10.1016/j.scitotenv.2006.11.029.
Stute, M., Zheng, Y., Schlosser, P., Horneman, A., Dhar, R.K., Datta, S., Hoque, M.A., Seddique, A.A., Shamsudduha, M., Ahmed, K.M., van Geen, A., 2007. Hydrological control of as concentrations in Bangladesh groundwater. Water Resour. Res. 43, W09417 https://doi.org/10.1029/2005WR004499.
Sun, J., Mailloux, B.J., Chillrud, S.N., van Geen, A., Thompson, A., Bostick, B.C., 2018. Simultaneously quantifying ferrihydrite and goethite in natural sediments using the method of standard additions with X-ray absorption spectroscopy. Chem. Geol. 476, 248–259. https://doi.org/10.1016/j.chemgeo.2017.11.021.
Swartz, C.H., Blute, N.K., Badruzzman, B., Ali, A., Brabander, D., Jay, J., Besancon, J., Islam, S., Hemond, H.F., Harvey, C.F., 2004. Mobility of arsenic in a Bangladesh aquifer: inferences from geochemical profiles, leaching data, and mineralogical characterization. Geochem. Cosmochim. Acta 68, 4539–4557. https://doi.org/10.1016/J.Gca.2004.04.020.
Thi Hoa Mai, N., Postma, D., Thi Kim Trang, P., Jessen, S., Hung Viet, P., Larsen, F., 2014. Adsorption and desorption of arsenic to aquifer sediment on the red river floodplain at nam Du, Vietnam. Geochem. Cosmochim. Acta 142, 587–600. https://doi.org/10.1016/j.gca.2014.07.014.
van Geen, A., Ahmed, E.B., Pitcher, L., Mey, J.L., Ahsan, H., Graziano, J.H., Ahmed, K.M., 2014. Comparison of two blanket surveys of arsenic in tubewells conducted 12 years apart in a 25 km^2 area of Bangladesh. Sci. Total Environ. 488, 484–492. https://doi.org/10.1016/j.scitotenv.2013.12.049, 489.
van Geen, A., Bostick, B.C., Thi Kim Trang, P., Lan, V.M., Mai, N.-N., Manh, P.D., Viet, P.H., Radloff, K., Aziz, Z., Mey, J.L., Stahl, M.O., Harvey, C.F., Oates, P., Weinman, B., Stengel, C., Frei, F., Kipfer, R., Berg, M., 2013. Retardation of arsenic transport through a Pleistocene aquifer. Nature 501, 204–207. https://doi.org/10.1038/nature12444.
van Geen, A., Zheng, Y., Goodbred, S., Horneman, A., Aziz, Z., Cheng, Z., Stute, M., Mailloux, B., Weinman, B., Hoque, M.A., Seddique, A.A., Hossain, M.S., Chowdhury, S.H., Ahmed, K.M., 2008. Flushing history as a hydrogeological control on the regional distribution of arsenic in shallow groundwater of the bengal basin. Environ. Sci. Technol. 42, 2283–2288. https://doi.org/10.1021/es702316k.
Zhang, H., Selim, H.M., 2008. Reaction and transport of arsenic in soils: equilibrium and kinetic modeling. In: Advances in Agronomy. Academic Press, pp. 45–115. https://doi.org/10.1016/S0065-2113(08)00202-2.
Zhang, H., Selim, H.M., 2005. Kinetics of arsenate Adsorption–Desorption in soils. Environ. Sci. Technol. 39, 6101–6108. https://doi.org/10.1021/es050334u.
Zheng, Y., van Geen, A., Stute, M., Dhar, R., Mo, Z., Cheng, Z., Horneman, A., Gavrieli, I., Simpson, H.J., Versteeg, R., Steckler, M., Grazioli-Venier, A., Goodbred, S., Shahnewaz, M., Shamsudduha, M., Hoque, M.A., Ahmed, K.M., 2005. Geochemical and hydrogeological contrasts between shallow and deeper aquifers in two villages of Araihazar, Bangladesh: implications for deeper aquifers as drinking water sources. Geochem. Cosmochim. Acta 69, 5203–5218. https://doi.org/10.1016/j.gca.2005.06.001.